Materiales de Construcción
Vol. 74, Issue 354, April-June 2024, e340
ISSN-L: 0465-2746
https://doi.org/10.3989/mc.2024.363223

Studying the hydration kinetics and mechanical-microstructural properties of Portland cements made with and without dredged sediment: experimental and numerical approaches

D.C. Chu[a,b]✉, M. Benzerzour[a,b], M. Amar[a,b], J. Kleib[a,b], N-E. Abriak[a,b], G. Potier[a,b], J. Nadah[c].

a. IMT Nord Europe, Institut Mines-Télécom, Centre for Materials and Processes, (Douai, France)
b. Univ. Lille, Institut Mines-Télécom, Laboratoire de Génie Civil et géo-Environnement, (Lille, France)
c. EQIOM Le LAB, CRT 1 Parc Vendôme, (Lesquin, France)
✉: duc.chinh.chu@imt-nord-europe.fr

Received 5 September 2023
Accepted 24 January 2024
Available on line 11 June 2024

ABSTRACT: This research focused on two objectives: (i) investigating the impacts of sediment substitution in the raw meal on the hydration and mechanical-microstructural properties of cement; (ii) assessing the reliability of CEMHYD3D code for modeling the properties of hydrated cement. The experimental results indicated that a maximum rate of sediment up to 7.55% had no impact on the formation of mineralogical phases of clinker, the hydration and mechanical-microstructural development of cement. The degree of hydration and strengths of cement made of sediment substitution were slightly higher than those of reference cement, whereas the critical diameter of pores of both hydrated cements was nearly identical. Comparing the modeling results with the experimental measurements showed good predictions for the degree of hydration, hydration heat as well as strength development. However, the formation of hemi-and mono-carboaluminate phases was not predicted in the model, and the porosity prediction was also limited to the capillary porosity.

KEY WORDS: Sediment; Cement; Clinker; Modeling; Hydration; CEMHYD3D.

Citation/Citar como: Chu DC, Benzerzour M, Amar M, Kleib J, Abriak N-E, Potier G, Nadah J. 2024. Studying the hydration kinetics and mechanical-microstructural properties of Portland cements made with and without dredged sediment: experimental and numerical approaches. Mater. Construcc. 74(354):e340. https://doi.org/10.3989/mc.2024.363223.

RESUMEN: *Estudio de la cinética de hidratación y propiedades mecánico-microestructurales de cementos Portland elaborados con y sin sedimento dragado: aproximaciones experimentales y numéricas.* Esta investigación se centró en dos objetivos: (i) investigar los impactos de la incorporación de sedimentos dragados sobre la hidratación y las propiedades mecánico-microestructurales del cemento; (ii) evaluar la confiabilidad del código CEMHYD3D para modelar las propiedades del cemento hidratado. Los resultados experimentales indicaron que un contenido máximo de sedimentos de hasta 7,55% no tuvo impacto en la formación de fases mineralógicas del clínker, la hidratación y el desarrollo mecánico-microestructural del cemento. El grado de hidratación y las resistencias del cemento obtenido a partir de la sustitución de sedimentos fueron ligeramente superiores a las del cemento de referencia, mientras que el diámetro crítico de los poros de ambos cementos hidratados fue casi idéntico. La comparación de los resultados de la modelización con los experimentales mostró buenas predicciones para el grado de hidratación, el calor de hidratación y el desarrollo de las propiedes mecánicas. Sin embargo, la formación de fases de hemi y monocarboaluminato no se predijo en el modelo, y la predicción de la porosidad también se limitó a la porosidad capilar.

PALABRAS CLAVE: Sedimento; Cemento; Clinker; Modelización; Hidratación; CEMHYD3D.

1. INTRODUCTION

Concrete has become the most manufactured product in the world in terms of volume, with approximately 5.3 billion m^3 produced per year (1, 2). Cement is one of the essential components used for the concrete production with about 3.6 billion tons produced in 2011 (3). However, cement production also has some adverse effects on the environment due to the large quantity of CO_2 emissions and massive consumption of natural resources such as limestone, clay and sand (1). Indeed, the production of a ton of Portland cement requires 1.5 tons of raw materials (4), so it can be seen that the cement industry consumed approximately 5.4 billion tons of raw materials in 2011. As the natural material deposits are limited, the need for a sustainable trade-off between cement production and natural resource consumption has become a veritable issue for the global cement industry in the 21st century. One of the potential materials studied for a partial substitution of conventional raw materials is dredged sediment. Sediment presents some advantages such as the large available quantity with approximately 300 Mm^3 dredged in Europe per year (5), and the chemical composition which consists of CaO, Al_2O_3, SiO_2 and Fe_2O_3 (6–8), which is in accordance with the need for cement production. Although recycling the sediment in the raw meal has been previously investigated in several studies (9–11), the information on the hydration kinetics and microstructure of these cements is still very limited. We also saw that in these studies, the cement hydration behavior was not precisely assessed due to the difference in mineralogical composition as well as the origin of the raw materials for the cement production.

Since cement hydration is a complex process that depends on numerous parameters such as the composition of the cement, temperature, curing time and relative humidity. A change in one of these parameters could modify the cement hydration and the mechanical-microstructural properties of the hydrated cement. Additionally, the experimental analyses often require time and many materials for preparation and testing. The numerical modeling of cement hydration is one of the most efficient ways to predict the properties of cement hydrated and save time and cost.

Nowadays, ever-improving computational models have facilitated the study of the hydration kinetics of cementitious materials. The computational models such as CEMHYD3D (12–16), VCCTL (17, 18), HYMOSTRUC (19, 20), HydratiCA (21) have accurately simulated the hydration kinetics as well as the relationship with the mechanical-microstructural development of Portland cement-based materials cured under the same conditions as in the experiment. The modeling results could provide a better understanding of cement hydration, which is useful not only for predicting the properties of hardened cement composites but also for developing an advanced design of cement-based materials (22). In addition, numerical simulation would save time and cost in comparison with the experiment (22, 23). For these reasons, the objectives of this study were to study the hydration behavior as well as mechanical-microstructural development of cement made from the sediment substitution in the raw meal via experiment and numerical simulation. The novelty of this study was the application of the CEMHYD3D model to numerically simulate the hydration of cement made from the waste substitution instead of cement made from analytical reagents used in previous studies. Numerous parameters of this model were modified to adapt to both cements in this study to simulate the cement hydration and predict all the fundamental properties of cement hydrated, including the hydration heat, the microstructure, and the strength. The modeling results could be used to rapidly investigate the influence of the composition of cement on the properties of cement hydrated. This could be applied in the practical to optimize the composition of cement in terms of the practical requirement. To achieve these objectives, we focused on the following aspects:

- Two clinkers/cements were produced in this study with the same targeted mineralogical composition. The first one is the reference produced from conventional raw materials only. The second one was made with a maximum amount of sediment incorporated in the raw meal. The hydration kinetics and mechanical-microstructural properties of both cements were studied by the experiment to investigate the potential influence of sediment on the quality of cement.
- The hydration kinetics as well as the development of mechanical-microstructural properties of both cements were modeled using CEMHYD3D code. The modeling results were also compared with the experimental results to investigate the ability and reliability of the CEMHYD3D code for the prediction of the properties of cement made with and without sediment substitution in the raw meal. Understanding the modeling results of CEMHYD3D code, we can accurately predict the hydration kinetics and the mechanical-microstructural developments of cement in a practical application, saving the time for the sample preparation and analyses cost.

2. MATERIALS AND METHODS

2.1. Raw materials and cement production process in the laboratory

In this study, two ordinary Portland cements (OPC) were made by grinding together clinker and gypsum in a laboratory ball mill. Two different clinkers were produced with and without sediment in the raw meal. The sediment used is fluvial sediment collected from the Air sur Lys region (hereafter ASL) in the North of

France. It was homogenized and dried at 105 °C until it reached a constant weight before characterization. Contrary to several previous studies (9, 10), which used analytical reagents as the raw materials, in this study, the raw materials used were limestone, clays, sand and iron oxide that were extracted from the natural quarries. They were also dried at 105 °C until a constant weight and ground to a smaller particle size than 200 µm before characterization. The chemical composition of all materials obtained using X-ray fluorescence (XRF) analysis is given in Table 1.

Based on the chemical composition of all raw materials as well as the targeted mineralogical composition of clinkers, two raw mixtures were formulated with and without sediment using the moduli values: LSF = 98, SR = 2.6 and AR = 1.45 respectively (24). The proportion of other raw materials in these mixtures must respect the following proportions: $\frac{LM1}{LM2+LM3}$=1.5 and $\frac{CLAY2}{CLAY1}$=1.5 as required by the industrial partner. In addition, the analysis of the consistency of raw meal made with different rates of sediment was also performed to determine the maximum incorporable rate of sediment in the raw meal. The raw meals were prepared by mixing the raw materials with the same amount of water (water-to-solid ratio of 0.3) for 5 minutes before being poured onto a flat surface. The consistency of raw meal was determined by measuring the diameter of pates, as illustrated in Figure 1.

Table 1. Chemical composition of all raw materials obtained by XRF analysis.

Materials	Sediment	Limestone 1	Limestone 2	Limestone 3	Clay 1	Clay 2	Sand	Iron oxide	Gypsum
Oxide (wt%)	ASL	LIM 1	LIM 2	LIM 3	CLY 1	CLY 2	SAN	IRO	GYP
SiO_2	65.15	5.3	9.5	6.0	48.7	60.6	88.3	2.2	1.95
Al_2O_3	7.35	1.9	3.7	1.2	20.6	14.9	4.8	0.3	0.33
Fe_2O_3	3.1	0.6	1.3	0.6	10.7	7.9	1.2	70.6	0.28
CaO	7.55	49.8	45.8	50.0	1.1	2.3	2.1	13.5	32.85
MgO	0.7	0.4	0.6	0.4	1.1	0.8	ND	2.2	0.34
Na_2O	0.85	ND	ND	ND	ND	ND	ND	ND	0
K_2O	1.65	0.4	0.9	0.2	1.5	1.3	0.3	0.1	0.08
SO_3	0.1	ND	ND	ND	ND	ND	ND	0.2	38.58
TiO_2	0.65	ND	0.1	ND	0.7	0.7	0.9	ND	0
P_2O_5	0.25	ND	ND	0.2	0.3	0.2	ND	ND	0
Mn_2O_3	ND	ND	ND	ND	ND	0.2	ND	0.7	0
ZnO	0.1	ND	ND	ND	ND	ND	0.1	ND	0
LOI	12.1	40.9	37.5	40.9	14.6	10.5	1.9	10.2	24.85
Total	99.5	99.3	99.4	99.5	99.3	99.4	99.6	98.7	99.28

Note: ND = not detected.

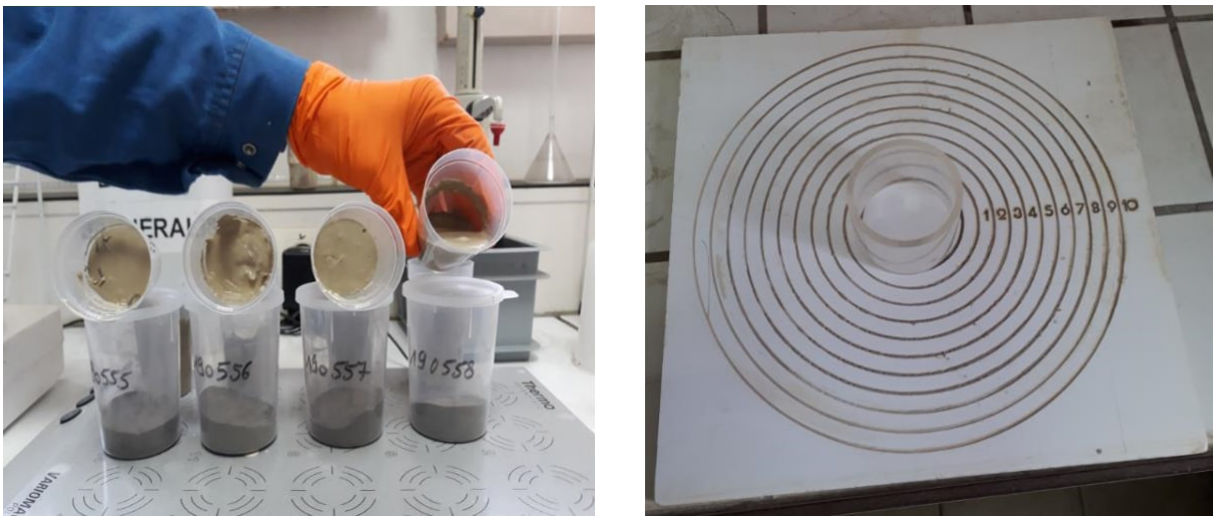

Figure 1. Consistency measurement of raw pates with different substitution rate of sediment.

Based on the chemical composition of raw materials as well as the consistency of raw pastes, the maximum incorporable rate of sediment in the raw meal is limited to 7.55%. This is very important for assuming an adequate content of water used for raw paste preparation before the clinkering. It should be noted that a greater water content was used, the energy consumption was greater, leading to an increase in the cost of the cement product. The economic efficacy and environmental impact of sediment substitution in cement production will be presented in our future paper. In this study, two cements were produced as follows: the first cement (OPC Ref cement) was produced from conventional raw materials only, and the second, OPC-Sed cement, was made with a maximum substitution rate of sediment up to 7.55%. The composition of two raw meals is given in Table 2.

Two clinkers were produced in this study according to the process described in a previous study (9). After the clinkering, the free lime content (CaO_{free}) of two clinkers was measured using the Schlafer-Bukolowki method (25). The chemical compositions of clinkers were measured using XRF analysis, while the mineralogical compositions were obtained using the Bogue formula (26) according to following Equations:

$$C_3S = 4.07*(CaO_{tot} - CaO_{free}) - 6.72*Al_2O_3 - 1.43*Fe_2O_3 \quad [1]$$

$$C_2S = 8.60*SiO_2 + 1.08*Fe_2O_3 + 5.07*Al_2O_3 - 3.07*(CaO_{tot} - CaO_{free}) \quad [2]$$

$$C_3A = 2.65*Al_2O_3 - 1.69*Fe_2O_3 \quad [3]$$

$$C_4AF = 3.04*Fe_2O_3 \quad [4]$$

Where:
CaO_{tot}, SiO_2, Al_2O_3 and Fe_2O_3 are the chemical compositions of clinker.
CaO_{free} is the content of free lime of clinker.
The chemical-mineralogical compositions of two clinkers are given in Table 3.

The CaO_{free} amount of both clinkers was less than the threshold value of 2% usually required in the cement industry (27). It also meant that the clinkering process was complete and that the cooling process did not lead to the decomposition of C_3S into C_2S and CaO_{free}. In addition, it can be seen that OPC-Sed clinker contained more C_3S and less C_2S content when compared with the reference clinker. This was principally due to the higher content of CaO and lower content of SiO_2 in OPC-Sed clinker.

Table 2. Composition of two raw meals with and without the sediment.

Raw meal	ASL (wt%)	LIM1 (wt%)	LIM2 (wt%)	LIM3 (wt%)	CLY1 (wt%)	CLY2 (wt%)	SAN (wt%)	IRO (wt%)
OPC Ref	0	52.08	17.36	17.36	3.18	4.78	4.31	0.93
OPC Sed	7.55	51.31	17.10	17.10	2.40	3.61	0.0	0.93

Table 3. Chemical-mineralogical composition of both clinkers.

Chemical composition	OPC Ref clinker	OPC-Sed clinker
SiO_2	21.05	20.52
Al_2O_3	5.22	5.58
Fe_2O_3	2.93	2.96
CaO	65.19	65.47
MgO	0.72	0.75
Na_2O	ND	ND
K_2O	0.71	0.86
SO_3	0.03	0.0
ZnO	0.03	0.04
P_2O_5	0.18	0.20
L.O.I	3.00	2.70
Total	99.40	99.44
Mineralogical composition	OPC Ref Clinker	OPC-Sed Clinker
C_3S	61.63	63.98
C_2S	15.76	12.23
C_3A	9.14	10.06
C_4AF	9.18	9.25
CaO_{free}	1.60	1.65

The influence of sediment substitution on the chemical composition of mineralogical phases was also investigated using the SEM-EDS technique. The clinker samples were cut into 2 mm thick slices, and then they were impregnated under vacuum using the epoxy. These samples were polished using diamond suspension, with deodorized petroleum used as lubricant. Between each step, isopropanol was used to clear these samples. They were kept for 2 days in a desiccator under vacuum to remove the remaining isopropanol before being coated with carbon to make the surface conductive for SEM-EDS analysis at high vacuum. The Hitachi S-4300SE/N operates with an accelerating voltage of 20 kV, and a current of 0.8 mA was used to measure 100 points for each mineralogical phase in different zones to obtain a representative result. The SEM images of OPC Ref and OPC Sed clinker are shown in Figure 2 (a, b).

The SEM result also indicated that the sediment substitution in the raw meal did not change the distribution and morphology of the phases of clinker. Indeed, the morphology of alite (C_3S) and belite (C_2S) in both clinker in this study is typical morphology for these phase as observed in a previous study (28).

The chemical composition of all four major phases of both clinkers obtained from SEM-EDS analysis is shown in Figure 3 (a, b, c, d) corresponding to C_3S, C_2S, C_3A, and C_4AF, respectively.

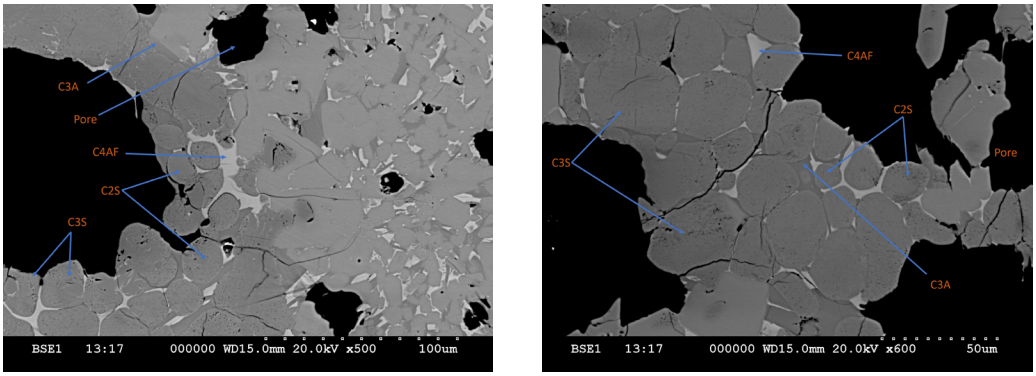

(a) (b)

Figure 2. SEM images of clinkers (a) OPC Ref clinker; (b) OPC Sed clinker.

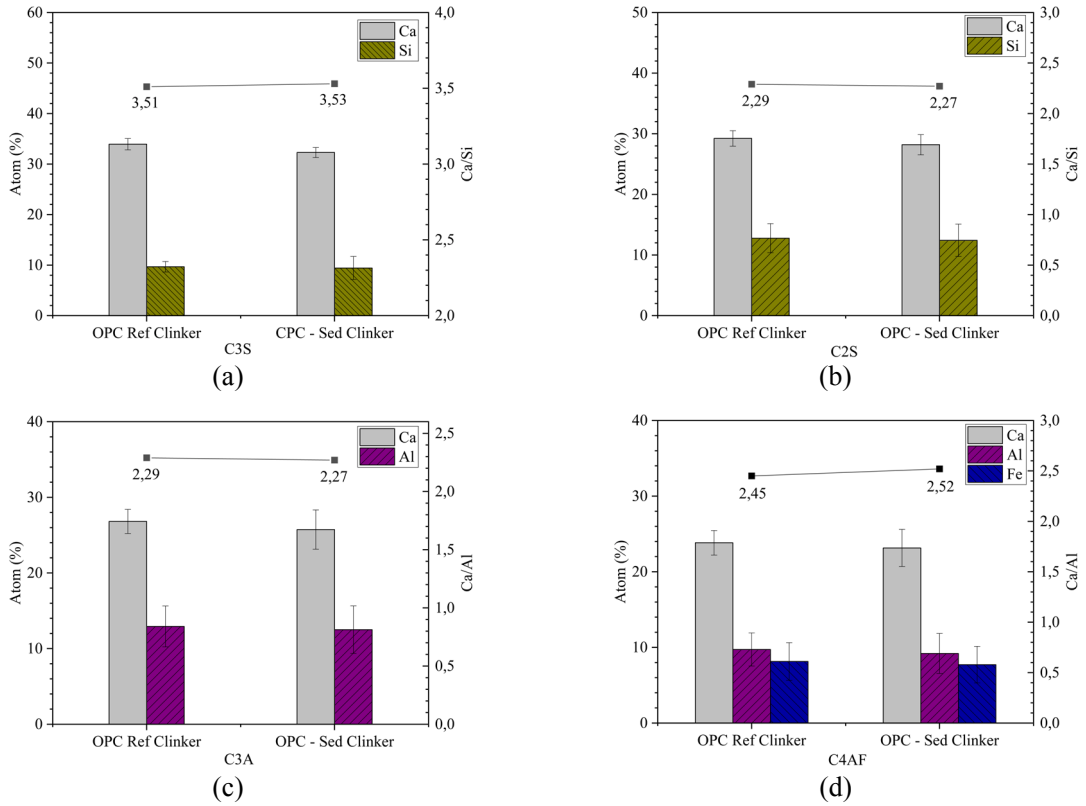

Figure 3. Chemical composition of four major phases of both clinkers measured by SEM-EDS analysis (a) C_3S; (b) C_2S; (c) C_3A; (d) C_4AF.

Observing the SEM-EDS result, it can be seen that the sediment substitution in the raw meal has not had a significant impact on the chemical composition of all four major phases. Indeed, the ratio of major elements in these mineralogical phases of both clinkers is nearly similar. This is interesting to investigate the cement quality made from the sediment substitution because the uptake of minor elements such as K^+, Na^+ or Mg^{2+} could modify the morphology of the mineralogical phase, in particular in the C_3S phase as described in a previous study (9). However, the ratio of major elements in all four major phases is slightly higher than the theoretical values of these phases found in the literature. For example, in the case of C_3S, the Ca/Si ratio obtained from the SEM-EDS analysis is 3.51, and 3.53 for OPC Ref Clinker, and OPC – Sed Clinker respectively, while the theoretical value is 3.0. The difference between the experimental value and the theoretical value can be due to numerous reasons, including the presence of foreign elements or the interaction of phases.

Gypsum was added to obtain a total SO_3 amount of 3.6% in both cements. This was an optimized sulfate content for a plain Portland cement hydration as defined in the NF EN 197-1 standard (29). Based on the chemical composition of gypsum and clinkers presented in Table 1 and Table 3 respectively, the mass proportion of each component of OPC Ref and OPC Sed cements is given in Table 4.

Table 4. Mass proportion of each component of both cements.

Cement	Clinker (%)	Gypsum (%)
OPC Ref	90.71	9.29
OPC Sed	90.64	9.36

Then, clinker and gypsum were ground using a ball-mill device until they achieved a Blaine surface of 4500 cm2/g.

2.2. Characterization methods

2.2.1. Characteristics of anhydrous cements

The particle size distributions (PSDs) of both anhydrous cements were measured using laser diffraction (COULTER type LS 13320 device) with isopropanol used as the dispersant. The specific density was also obtained using the helium pycnometer Accupyc 1330 device, while the specific surface area was measured by the Blaine surface method (30) and the BET method (Brunaer-Emmett-Teller). The initial setting time as well as water demand of both cements were determined according to the NF EN 196-3 standard (31) using a Vicat instrument. All characteristics of both anhydrous cements are given in Table 5.

Table 5. Characteristics of two anhydrous cements.

Properties	OPC Ref	OPC – Sed
Density (g/cm^3)	3.1	3.1
Blaine specific surface area (cm^2/g)	4450	4460
BET specific surface area (m^2/g)	1.46	1.47
d_{10}(µm)	1.48	0.99
d_{50}(µm)	14.18	14.56
d_{90}(µm)	32.16	31.62
Water demand (%)	30.03	30.05
Initial setting time (minutes)	180	180

2.2.2. Hydration kinetics and mechanical-microstructural development of hydrated cements

Contrary to several previous studies (11, 32), which investigated the cement hydration through the hydration heat and compressive strength development only, in this study, the hydration kinetics and mechanical-microstructural properties of OPC Ref and OPC-Sed cements were studied using numerous experimental analyses, including the advancement of hydration and hydration heat of pastes, compressive strength, and porosity evolution of mortar samples.

The advancement of hydration reactions with time could provide information on the hydration behavior of cement. The results obtained in a previous study (33) indicated that the measurement of chemically bound water was the best method for the determination of the degree of hydration of cement (hereafter DoH) thus, in this study, the DoH of cements was determined using thermogravimetry analysis (TGA) based on the measurement of chemically bound water amounts during cement hydration. Two cement pastes were prepared with a water-to-cement ratio of 0.5, and cured under saturated conditions at a constant temperature of 20 °C until specific ages for measurement. At the time of testing, the cement paste samples were crushed into fine particles (<63 µm), then they were directly analyzed in a TG instrument (Netzsch STA 409). TGA was performed according to the process described in a previous study (33). The DoH of hydrated cements was calculated according to Equation [5]:

$$\alpha(t) = \frac{Wn\,(t)}{Wn(\infty)} \qquad [5]$$

Where:
α(t): Degree of hydration of cement at time t.
W_n(t): Chemically bound water amount of cement paste at time t.
W_n(: Ultimate chemically bound water amount corresponding to the complete hydration of cement paste.

The TGA curve and DTG curve of OPC Ref cement paste after 28 days of hydration are presented in Figure 4 (a, b) respectively.

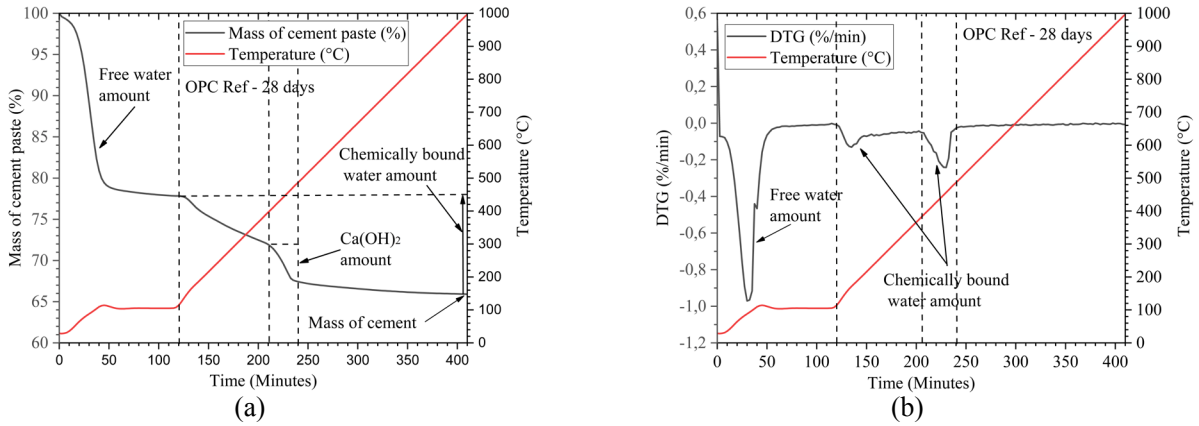

Figure 4. (a) TGA curve of OPC Ref cement paste after 28 days of hydration; (b) DTG curve of OPC Ref cement paste after 28 days of hydration.

Based on the TGA curve and DTG curve, it can be seen that the loss of mass of cement paste in the range of 40 °C to 105 °C corresponds to the mass of evaporable water (free water), while the chemically bound water content is obtained by measuring the loss of mass of the sample between 105 °C and 1000 °C. The $Ca(OH)_2$ amount could be determined by measuring the mass loss of the sample in the range of 400 °C to 500 °C. Table 6 summarizes the mass loss of each sample corresponding to the different temperature ranges.

The chemically bound water amount of cement paste could be determined from the sample mass loss according to Equation [6]:

$$W_n(t) = \frac{\Delta m\ sample\ (105\ °C - 1000\ °C)(t)}{m\ sample\ (1000°C)(t)} * 100 \qquad [6]$$

The ultimate chemically bound water amount of cement was estimated using the method proposed by NIST (National Institute of Standards and Technology) as given in the work (34). The principle is to estimate the ultimate chemically bound water amount of individual phase when it totally reacts with water. In addition, in a previous study (33), we used three different methods to determine the degree of hydration (DoH) of cement pastes. The results indicated that the measurement of the ultimate chemically bound water amount is the best method for determining the DoH of Portland cement. For this reason, in this study, the DoH of both cement pastes was determined by measuring the chemically bound water amount. Based on the ultimate chemically bound water amount of individual phase, we can estimate the ultimate chemically bound water amount of cement according to Equation [7]:

$$W_n(\infty) = W_{nC3S}(\infty)*(\%C_3S) + W_{nC2S}(\infty)*(\%C_2S) + W_{nC3A}(\infty)*(\%C_3A) + W_{nC4AF}(\infty)*(\%C_4AF) + W_{nCaOfree}(\infty)*(\%CaO_{free}) \qquad [7]$$

Where:
$W_{nC3S}(\infty)$, $W_{nC2S}(\infty)$, $W_{nC3A}(\infty)$, $W_{nC4AF}(\infty)$, $W_{nCaOfree}(\infty)$ is the ultimate chemically bound water amount of C_3S, C_2S, C_3A, C_4AF and CaO_{free} respectively.

From the mineralogical composition of clinker and the mass proportion between gypsum and clinker in both cements given in Table 3 and Table 4 respectively, the mineralogical composition of both cements could be easily computed. Table 7 presents the mineralogical composition as well as $W_n(\infty)$ value of both cement.

The heat release during hydration was monitored using isothermal conduction calorimetry performed at a constant temperature of 20°C. For this measurement, cement paste was prepared with a water-to-cement ratio of 0.5 (W/C=0.5) according to the process described in the previous study (7, 9). After mixing for 2 min at 1600 rpm, 10g of paste was poured into a cell, which was then sealed and placed in the calorimeter. The heat liberated from the cement hydration reactions was measured for up to 70h.

X-ray diffraction (XRD) analysis was used to identify the anhydrous cement phases as well as the

Table 6. Mass loss of each sample corresponding to the different temperature range.

Mass loss	2 days		14 days		28 days	
	OPC Ref	OPC Sed	OPC Ref	OPC Sed	OPC Ref	OPC Sed
40 °C-105 °C	26.2	26.57	23.01	22.97	21.82	21.68
105 °C-1000 °C	7.87	8.26	11.56	11.74	12.77	13.08
Mass of cement	65.93	65.17	65.43	65.29	65.41	65.24

Table 7. Mineralogical composition and Wn(∞) value of both cements.

Phase	$W_{phase}(\infty)$ per gram	Mineralogical composition		$W_n(\infty)$ of cement (g/100 g of anhydrous cement)	
		OPC Ref	OPC - Sed	OPC Ref	OPC - Sed
C_3S	0.24	57.45	59.68	13.79	14.32
C_2S	0.21	14.69	11.41	3.08	2.39
C_3A	0.4	8.52	9.38	3.41	3.75
C_4AF	0.37	8.56	8.63	3.16	3.19
CaO_{free}	0.33	1.49	1.54	0.49	0.51
Gypsum	-	9.29	9.36	-	-
Total		100	100	23.93	24.17

hydration products of two cement pastes over time. The hydration of cement pastes was stopped using the solvent exchange method (isopropanol solvent) (35). Cement pastes were immersed in isopropanol for 3 days, then stored in a desiccator under vacuum for 7 days. The hydration-stopped pastes were ground to obtain a smaller particle diameter than 40 µm. The powders were analyzed using a Bruker D2 Advance diffractometer, which is equipped with Cu radiation, λ = 1.5406 Å. The measurement was performed at 40 kV-40 mA with the 2θ angle scanned from 5° to 80°.

The mechanical development was investigated by measuring the compressive strength of standard mortars. Samples (40 x 40 x 160 mm^3) were prepared according to the NF EN 196-1 standard (36) and cured under saturated conditions at a constant temperature of 20 °C. The compressive strength of mortars was measured after 1, 2 and 28 days of curing, respectively using an INSTRON 5500R device that has a maximum applicable load of 150 kN and a displacement rate of 144 KN/min.

The microstructure development of hydrated cement over time was monitored using the Mercury Intrusion Porosimetry (MIP) method. For MIP measurement, mortar samples were cut into small pieces of 1 x 1 x 1 cm^3 and immersed in isopropanol for 3 days to stop the hydration. Samples were then stored in a desiccator for at least 7 days before measurement. In this study, the total porosity and pore size distribution of samples were measured after 1 and 28 days of hydration using an Autopore IV device. The instrument has a maximum applicable pressure of 200 MPa, and is able to detect a minimum pore diameter of 6 nm.

In addition, the pore structure could be studied measuring the capillary porosity according to BS 1881 Pt. 124 (37) based on the DoH of cement. The calculated capillary porosity of mortar was obtained according to Equation [8]:

$$P = \frac{\frac{w}{c} - 0.36\alpha(t)}{\frac{w}{c} + 0.32} * V(\%)_{\text{cement paste in the mortar}} \quad [8]$$

Where P is the calculated capillary porosity of mortar
α(t) is the degree of hydration of cement.
V(%) is the percentage of cement paste by volume in the mortar.
W/C is the water-to-cement ratio of mortar.

2.2.3. Numerical simulation of cement hydration

In this part, the hydration and mechanical-microstructural properties of cements were studied via a three-dimensional microstructure generated in CEMHYD3D. This model, developed by D.P.Bentz at NIST, has been employed in several previous studies in order to study the properties of hydrated cement (13, 14, 38). The CEMHYD3D was used with the cellular automate algorithm to generate the virtual cement pastes from the characteristics of anhydrous cements, including the mineralogical composition, granulometry (PSDs), specific density as well as water-to-cement ratio used in the prepared mixtures. Firstly, the PSDs data of both anhydrous cements were used to place the particles of virtual cements from largest to smallest diameters at random locations in a 3-D computational volume of 100 x 100 x 100 μm^3. The volumetric proportion of all cement phases was converted from their mass fraction data given in Table 7 with the hypothesis that a low CaO_{free} amount in the clinker had no significant effect on the hydration kinetics of cements. Table 8 presents the PSDs of two cements measured in the experiment and simulated in CEMHYD3D.

The volume proportion of mineralogical phases of two cements as well as the water-to-cement ratio of virtual pastes obtained from the experimental measurement and numerical simulation in CEMHYD3D are given in Table 9.

In general, comparing the experiment with the modeling results indicated good agreement for the two cement pastes. However, it can be seen that the PSDs of both cements measured in the experiment were slightly greater than those of the two virtual cements.

Table 8. PSDs of OPC Ref and OPC-Sed cement obtained from the experiment and numerical simulation in the CEMHYD3D.

	OPC Ref		OPC - Sed	
Diameter of particles (μm)	Mass fraction (%) (Exp)	Mass fraction (%) (CEMHYD3D)	Mass fraction (%) (Exp)	Mass fraction (%) (CEMHYD3D)
1	10.480	10.660	10.49	10.262
3	2.450	2.492	2.29	2.243
5	5.360	5.447	5.46	5.339
7	7.270	7.386	7.40	7.243
9	8.020	8.124	8.15	8.018
11	8.070	8.282	8.17	8.086
13	7.640	7.874	7.76	7.564
15	7.000	7.299	7.14	6.837
17	6.230	6.502	6.37	6.497
19	5.460	5.647	5.64	5.642
21	4.730	5.038	5.01	5.034
23	4.140	4.893	4.55	4.888
25	3.710	4.186	4.18	4.182
29	6.500	6.568	7.29	6.562
33	7.250	9.604	7.01	4.798
37	3.010	0.000	2.11	6.806
49	2.65	0.000	0.97	0.000
Total	99,97	100	99.99	100

Table 9. Mineralogical composition of OPC Ref and OPC-Sed cements obtained from the experimental measurement and numerical simulation in CEMHYD3D.

Phases	OPC Ref			OPC - Sed		
	Exp (%)	CEMHYD3D		Exp (%)	CEMHYD3D	
		Pixels	% Volume		Pixels	% Volume
C_3S	0.5708	223945	0.5704	0.5924	235642	0.5943
C_2S	0.1428	56692	0.1444	0.1108	43963	0.1109
C_3A	0.0897	35493	0.0904	0.0986	38991	0.0983
C_4AF	0.0731	28712	0.0731	0.0737	29362	0.0740
Gypsum	0.1234	47776	0.1217	0.1244	48572	0.1225
Total	1.00	392618	1.00	1.00	396530	1.00
W/C	0.5	0.499		0.5	0.491	

Finally, the hydration of these virtual cement pates was simulated under the same conditions used in the experiment. During hydration simulation, the voxels of cement phases can dissolve, diffuse, and react to form hydration products. For all of the simulations performed using the CEMHYD3D, the conversion factor was used to convert the model cycles into read time. It was calculated using the DoH experimental value of cement pastes measured by TG analysis after 2 days of hydration to calibrate the modeling result as described in a previous study (9). From the output data of the model, numerous aspects of hydrated cement could be studied, such as the DoH of cement and individual cement phases, the evolution of hydration

products, hydration heat, and microstructural development. Power's empirical relation (Equation [9]) was used in the CEMHYD3D to predict the compressive strength (39).

$$\sigma_c(t) = \sigma_0\left(\frac{0.68\,\alpha(t)}{0.32\alpha(t)+\frac{W}{C}}\right)^n \qquad [9]$$

Where:
α is the degree of hydration of cement.
$\sigma_c(t)$: Compressive strength of mortar at time t (days).
σ_0: Compressive strength of mortar when the capillary porosity is zero. It was calculated from the experimental compressive strength of mortars measured after 2 days.
n: Coefficient depending on the cement type.
W/C: Water to cement ratio used in the mortar.

3. RESULTS AND DISCUSSIONS

3.1. Hydration kinetics

Figure 5 presents the model prediction and the experimental result for DoH of OPC Ref and OPC-Sed pastes. The result indicated that the DoH of OPC-Sed cement was always slightly higher than the reference cement at any time of testing. The DoH of OPC Ref and OPC-Sed cements increased with time and reached 0.81 and 0.815, respectively after 28 days of hydration. This confirmed that the sediment substitution level of 7.55% in the raw meal did not impact the reactivity of the mineralogical phases of cement.

For the modeling result, in general, CEMHYD3D provided a good prediction of DoH for both cements when compared with the experiment. As the experimental result, the DoH of OPC-Sed cement predicted in the CEMHYD3D was also slightly higher than that of OPC Ref cement. However, it can be seen that for the two cement pastes, the DoH predicted in the CEMHYD3D was slightly higher than that measured by the experiment with the DoH values of 0.835 for OPC Ref cement and 0.852 for OPC-Sed cement after 28 days of hydration. This can be attributed to the difference between the cement particle size measured by the experiment and the simulation in the model as indicated in Table 7. Indeed, in cement hydration, the hydration rate of coarser cement is generally lower than that of finer cement (40).

The cumulative hydration heat of OPC Ref and OPC-Sed cements, measured by isothermal conduction calorimetry and modeled in CEMHYD3D is shown in Figure 6. The experimental result indicated that the hydration kinetics of both cements were nearly similar when we compared the curve shape as well as the cumulative heat. As a result of the DoH measurement, the hydration heat of OPC-Sed cement was slightly higher than that of OPC Ref cement. Indeed, after 72h of hydration, the cumulative hydration heat

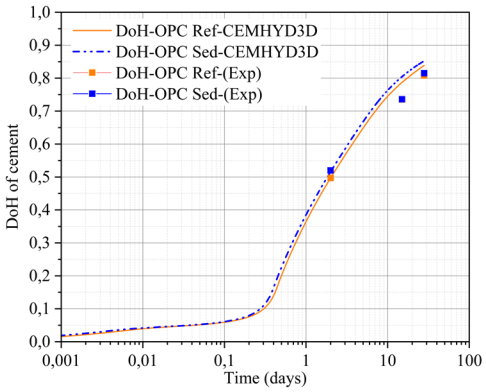

Figure 5. Experimental (data points) and model predicted (line) degree of hydration for OPC Ref and OPC-Sed, W/C= 0.5, hydrated under saturated conditions at 20° C.

of OPC Ref cement was 291.75 (KJ/kg), while OPC-Sed cement achieved 310.84 (KJ/kg).

Furthermore, it can be seen that the model prediction for the cumulative hydration heat was in nearly perfect agreement with the experimental measurement for both cement pastes. Indeed, the cumulative hydration heat predicted in the model was 283.80 (KJ/kg) for OPC Ref cement and 305.44 (KJ/kg) for OPC-Sed cement after 72h of hydration. The model also indicated that the heat liberated from the hydration of OPC-Sed cement was greater than that of OPC-Ref cement, with a cumulative heat of 435.64 (KJ/kg) for OPC Ref cement and 460.51 (KJ/kg) for OPC-Sed cement after 28 days of hydration. However, the mode appeared to slightly overestimate the heat released at very early ages (several minutes), while slightly underestimating it within 20-30 h for both cement pastes. The difference at very early ages was very likely due to the capability of an isothermal calorimetry device which was able to measure the hydration heat after approximately 5 minutes only.

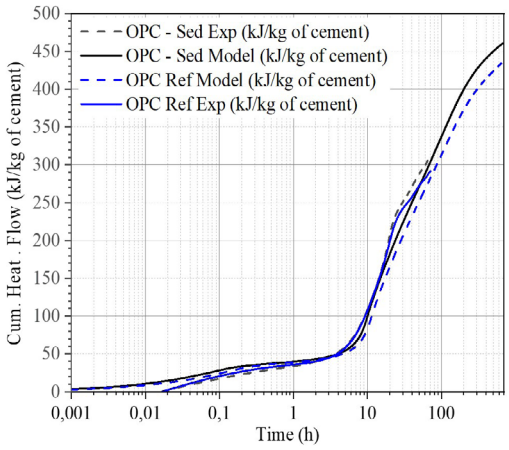

Figure 6. Hydration heat of OPC Ref and OPC-Sed cement obtained from the isothermal conduction calorimetry analyses and the simulation using the CEMHYD3D model.

The heat evolution curve and hydration progress of all individual cement phases of both cement pastes were studied to better understand the contribution of each cement phase to the hydration heat peak. The heat flux curve liberated from the hydration of both cements is also shown in Figure 7, while the hydration progress of all individual cement phases as a function of time predicted in the CEMHYD3D is highlighted in Figure 8 (a, b) corresponding to OPC Ref and OPC-Sed cement pastes respectively.

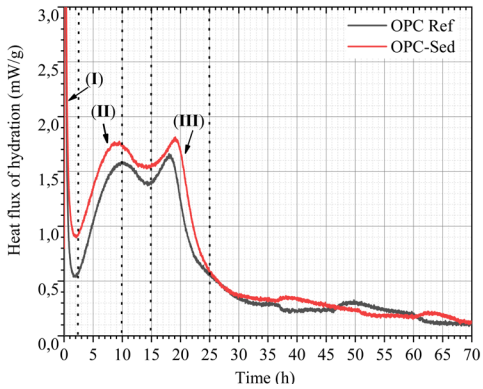

Figure 7. Heat flux of hydration of OPC Ref and OPC-Sed cement measured by isothermal conduction calorimetry.

The hydration heat curve of both cements may be distinguished in several stages, and in each stage, the contribution of individual cement phases on the hydration heat could be clearly investigated.

- Stage (I): The hydration reactions of both cements started immediately after contact with water, and the heat released in this stage can relate to the hydration of free lime, gypsum, and C_3A (35). Observing the hydration progress of individual cement phases shown in Figure 8 (a, b) also indicated that the hydration heat obtained in this stage had the origin from the hydration of gypsum, C_3A and C_4AF phases. In addition, the duration of the first peak simulated in the CEMHYD3D was much shorter, which was also in accordance with the observation in the experiment (41). After the pre-induction period, it can be seen that the hydration rate slowed significantly in the induction period, and thus the heat released in this period was also significantly reduced.
- Stage (II): After the induction period, the hydration rate of all individual cement phases increased again in the acceleration period. The modeling result presented in Figure 8 (a, b) showed that the duration of this period was between 3-15h. In this stage, the hydration rate of the C_3S phase was strongly higher than that of other phases, so the hydration heat released was principally associated with the hydration of the C_3S as the results found in the experiment (41).
- Stage (III): After the acceleration period, the hydration heat liberated started to slow down gradually. The decrease in hydration heat can be attributed to decreasing the hydration rate of the C_3S as observed in Figure 8 (a, b). However, in the case of our cements, after decreasing the hydration heat, the third heat peak was observed between 15h and 20h. Based on the modeling result, this increase in the hydration heat peak could be associated with increasing the hydration rate of the C_3A phase. Indeed, as observed in Figure 8 (a, b) for the two cement pastes, at this stage, a significant fraction of gypsum was consumed, which led to an increase in the hydration rate of the C_3A and the formation of ettringite (42). Experimentally, the hydration of the C_3A phase and the formation of ettringite liberated energy of 1670 kJ/kg and this heat was much higher than that released from the hydration of the C_3S phase (520 kJ/kg) (41).

In general, the hydration progress of individual cement phases over time simulated in CEMHYD3D for the two cement pastes was in accordance with the experimental observations (43-45). For the calcium silicate phases, the model prediction indicated that the C_3S hydration started much earlier and faster than

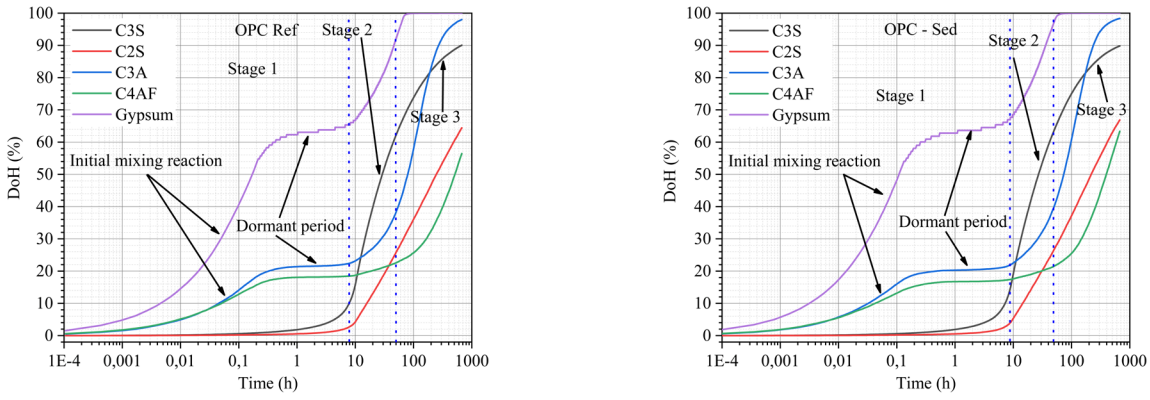

Figure 8. Degree of hydration of individual cement phases of cement simulated in CEMHYD3D with time. (a) OPC Ref cement; (b) OPC – Sed cement.

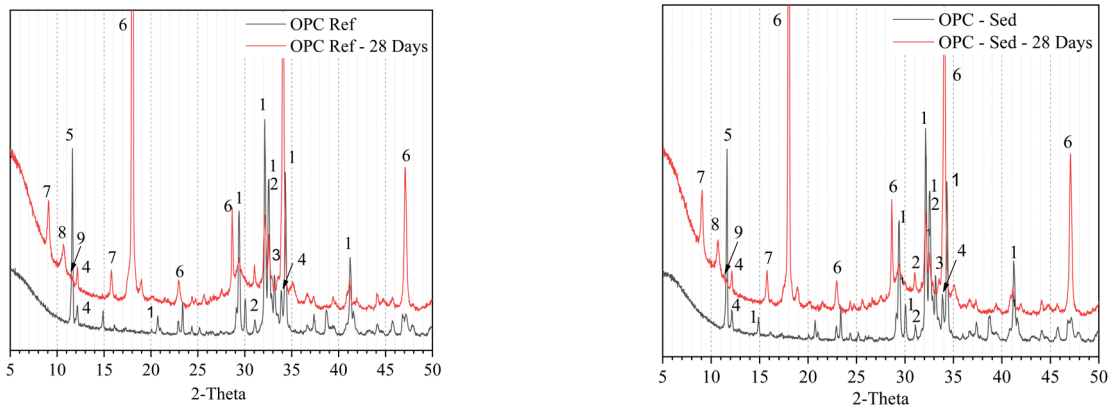

Figure 9. XRD patterns of anhydrous cement and after 28 days of hydration. (1) C_3S; (2) C_2S; (3) C_3A; (4) C_4AF; (5) Gypsum; (6) $Ca(OH)_2$; (7) Ettringite; (8) Hemi-carboaluminate; (9) Mono-carboaluminate. (a) OPC Ref cement; (b) OPC – Sed cement.

that of the C_2S phase. Indeed, more than 45% of the C_3S phase has reacted after 1day and about 90% after 28 days, while for the C_2S phase, the hydration rates were 20% and 68%, respectively at the same time. For the aluminate phases (C_3A and C_4AF), it can be seen that the hydration kinetics of the C_3A and C_4AF phases were similar, however the hydration rate of the C_4AF was much lower than that of that of the C_3A phase at long-term.

The hydration products of OPC Ref and OPC-Sed cements as a function of time identified using XRD analysis are shown in Figure 9 (a, b) respectively. The XRD patterns indicated that all hydration products of hydrated OPC-Sed cement were similar to those formed in hydrated OPC Ref cement. In the two cement pastes, the $Ca(OH)_2$ amount has increased with a decrease in the calcium silicate amount (C_3S, C_2S). However, the hydration rate of C_3S was much higher than that of the C_2S phase when we observed the peak magnitude of both phases. After 28 days of hydration, total gypsum and C_3A phases were consumed, while C_4AF phase was still detected. It appeared in accordance with the modeling result as shown in Figure 8 (a, b), which also indicated that the hydration kinetics of cement phases were not identical.

In addition, it can be seen that in the two cement pastes, C-S-H gels were not identified by XRD analysis due to their amorphous structure (44, 45). Hemi-carboaluminate (10.8°-2θ) and a low amount of mono-carboaluminate (11.7°-2θ) (46–49) were identified, while mono-sulfoaluminate (9.8°-2θ) was not detected. In Portland cement hydration, mono-sulfoaluminate was produced from the reaction between ettringite and excess of C_3A phase according to Equation [10], while hemi-carboaluminate and mono-carboaluminate were formed from the reaction between ettringite and calcite as described in Equation [11] and Equation [12] respectively (39). Moreover, calcite can to stabilize ettringite against the conversion to mono-sulfoamuminate (39, 49). Thus, the presence of these phases in the two cement pastes could be attributed to the following reaction series. First, the CO_2 in the atmosphere reacted with Portlandite to form calcite ($CaCO_3$). Then, a part of the calcite reacted with ettringite to form hemi-carboaluminate and mono-carboaluminate.

$$2C_3A + C_6A\underline{S}_3H_{32} + 4H \rightarrow 3CA\underline{S}H_{12} \text{ (Mono-sulfoaluminate)} \quad [10]$$

$$C_3A + 0.5C\underline{c} + 0.5CH + 11.5H \rightarrow C_4A\underline{c}0.5H_{12} \text{ (Hemi-carboaluminate)} \quad [11]$$

$$C_3A + C\underline{c} + 11H \rightarrow C_4A\underline{c}H_{11} \text{ (Mono-carboaluminate)} \quad [12]$$

The XRD patterns of OPC Ref and OPC Sed paste after 28 days of hydration are shown in Figure 10. It can be seen that the magnitude of the peaks in both XRD patterns is nearly similar. This result also confirmed that the sediment substitution did not influence the hydration behavior of cement, as indicated in the previous analyses.

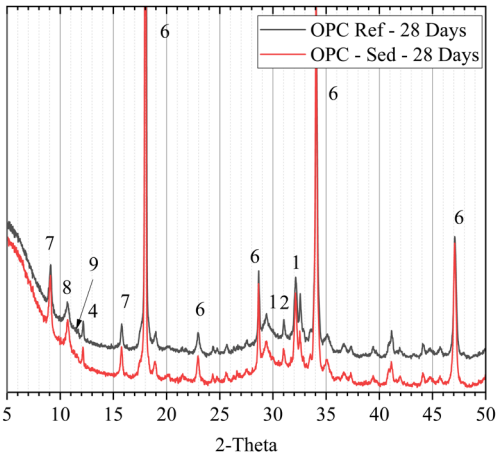

Figure 10. XRD patterns of OPC Ref and OPC Sed paste after 28 days. (1) C_3S; (2) C_2S; (4) C_4AF; (6) $Ca(OH)_2$; (7) Ettringite; (8) Hemi-carboaluminate; (9) Mono-carboaluminate.

The amount evolution of hydration products over time predicted in the CEMHYD3D is presented in Figure 11 (a, b) for OPC Ref and OPC-Sed cements respectively. For the two cement pastes, the modeling result also indicated an increase in Portlandite content with a decrease of anhydrous calcium silicate amount (C_3S, C_2S) as shown in Figure 8 (a, b) and Figure 9 (a, b). Contrary to the XRD analysis result, CEMHYD3D could predict the content of C-S-H gels formed in the two hydrated cements. As expected, the C-S-H gels were the primary hydration product with a volume fraction greater than 50% in the two cement pastes after 28 days of hydration. The model result showed that the formation of $Ca(OH)_2$ started later than that of C-S-H and it started to form at the end of the induction period as observed in the experiment (43). However, it can be seen that in the CEMHYD3D, the content of ettringite decreased with increasing the content of mono-sulfoaluminate when the total gypsum was consumed. Additionally, the presence of a combination of hemi-carboaluminate and mono-carboaluminate hydrates was not predicted. This was contrary to the result obtained in the XRD analysis. The difference between the experiment and the model result can be explained the fact that the CEMHYD3D did not consider the reaction between CO_2 and $Ca(OH)_2$, which led to the formation of calcite, which had two effects on the cement hydration as indicated above.

3.2. Mechanical-microstructural development

The compressive strengths of OPC Ref and OPC-Sed mortars measured in the experiment and predicted in the CEMHYD3D are shown in Figure 12. The strengths of OPC-Sed mortar were slightly higher than those of OPC Ref at any time of testing. The compressive strengths of OPC Ref and OPC-Sed mortars were 55.08 MPa and 56.57 MPa respectively after 28 days of curing, and they could be classified as CEM I 52.5 according to the NF EN 197-1 (29). Based on this result, we also confirmed that a sediment substitution rate up to 7.55% had no significant influence on the mechanical properties of hydrated cement.

For the modeling result, it can be seen that there is a perfect agreement between the experiment and prediction for the compressive strengths of mortars at early ages (1, 2 days). As the experimental result, the strengths of OPC-Sed mortar predicted by CEMHYD3D were also slightly higher than those of OPC Ref mortar. However, comparing with the experimental strength obtained at 28 days, the model appeared to slightly overestimate the compressive strength of both mortars. This gap in the prediction can be attributed to the slightly higher value of DoH predicted in the CEMHYD3D compared with the experiment at long-term as shown in Figure 5. Indeed, the compressive strength was predicted using the gel-space ratio theory as described in Equation [5], so increasing the DoH of cement led to increasing the strength of mortar predicted in the CEMHYD3D.

The porosity evolution as a function of time of OPC Ref and OPC-Sed mortars obtained from the experimental measurement and numerical simulation is presented in Figure 13 (a, b) respectively. This experimental result indicated that the porosity decreased with time, from 16.05% at 1 day to 12.76% at 28 days for OPC Ref mortar and from 15.78% at 1 day to 12.88% at 28 days for OPC-Sed mortar. For the modeling result, it can be seen that for the two mortars, the MIP measured porosity was similar to the CEMHYD3D model prediction at early age but much higher at long-term (28 days). This gap could be attributed to the following possibilities: (1) the dimension of pixels in CEMHYD3D was 1 x 1 x 1 μm^3, thus this model can measure the pores with a diameter $\geq$ 1 µm only, while the pore diameter determined by the MIP method included the small pores down to 0.006 µm

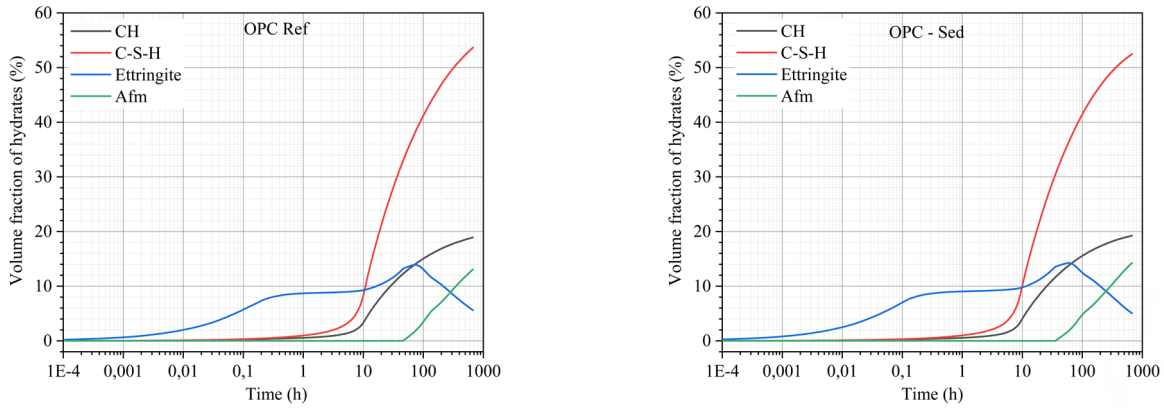

(a) (b)

Figure 11. Evolution with time of the volume fraction of hydration products produced from the hydration of cements simulated in CEMHYD3D, (a) OPC Ref cement; (b) OPC-Sed cement.

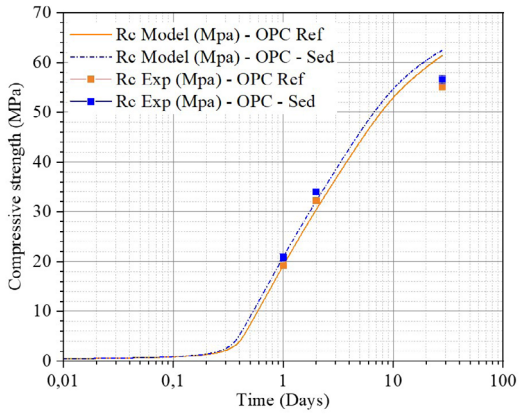

Figure 12. Experimental (date points) and model predicted (line) compressive strength development for OPC Ref and OPC-Sed mortar made with W/C=0.5, under saturated condition at 20° C.

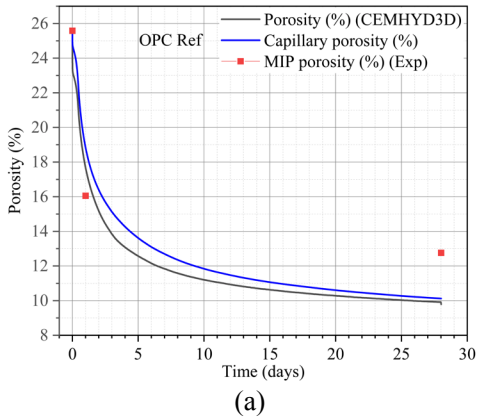

(a)

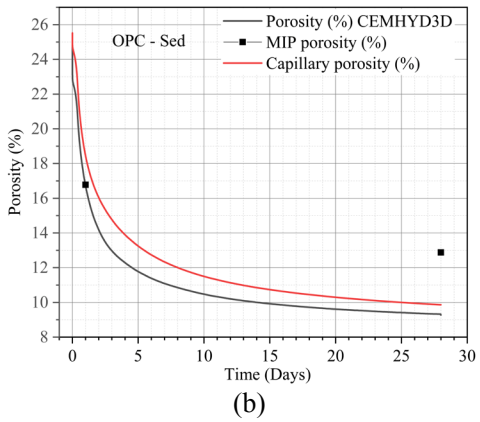

(b)

Figure 13. Porosity of mortars as a function of time measured experimentally, predicted in CEMHYD3D and calculated by the model (a) OPC Ref mortar; (b) OPC-Sed mortar.

(50); (2) high pressures of mercury in the MIP method might have damaged the pore structure leading to the increase in porosity (51).

Figure 14 presents the pore size distribution of both mortars measured by the MIP method after 1 and 28 days of hydration in order to verify the hypothesis above. As expected, for the two mortars, the pore diameter measured by the MIP method was much smaller than 1 µm, which explained why the MIP measured porosity was much higher than that predicted in the CEMHYD3D. However, the CEMHYD3D provided a good prediction of porosity when compared with the capillary porosity calculated according to Equation [4] for the two mortars. This is likely associated with the pore diameter that could be measured by Equation [4]. Indeed, it allowed determining the capillary porosity only in the size range of 0.01 to 10 µm (51). The diameter of these pores was much greater than the smallest diameter of pore determined by the MIP method. Thus, it explained why the porosity predicted in the CEMHYD3D was relatively similar to the capillary calculated porosity. These results indicated that the CEMHYD3D can be used to study the microstructure of Portland cement-based materials, but the porosity was limited to the capillary porosity. In addition, based on the results presented in Figure 9 (a, b) and Figure 10, we could also confirm that a sediment substitution rate up to 7.55% in raw meal had no impact on the durability of hydrated cement when we compared the total porosity as well as the critical diameter of two mortars.

4. CONCLUSIONS

The objectives of this study were to investigate the hydration and mechanical-microstructural properties of cement made from sediment substitution in the raw meal through experimental analyses and numerical simulation. Based on the experimental and numerical results available, the following conclusion can be drawn:

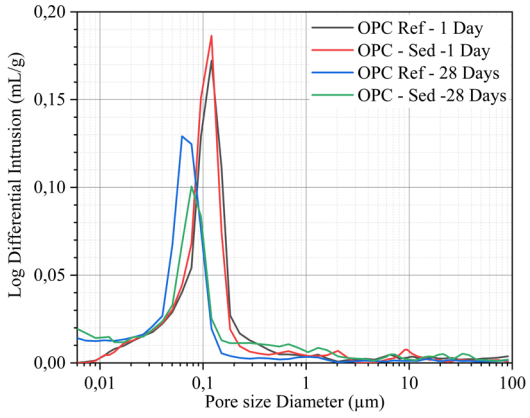

Figure 14. Pore size distribution of both mortars with time obtained from the experimental measurement (MIP method).

(1) Based on the chemical composition of the raw material as well as the consistency of raw pastes, the maximum incorporable rate of sediment in the raw meal is limited to 7.55%. A sediment substitution rate up to 7.55% in the raw meal had no impact on the formation of mineralogical phases of clinker as well as the properties of hydrated cement including the degree of hydration, strength and microstructure, when compared with the reference cement. The chemical composition of all four major phases of both clinkers obtained from the SEM-EDS analysis is nearly similar. The average ratio of major elements in all mineralogical phases measured by SEM-EDS analysis is slightly higher than the theoretical values. Indeed, the average ratio of the C_3S phase is 3.51 and 3.53 for OPC Ref clinker, and OPC-Sed clinker respectively, while the theoretical value is 3.0.
(2) The reactivity and compressive strengths of OPC-Sed cement were slightly higher than those of the reference cement at any time. After 28 days of hydration, the DoH of OPC Ref and OPC-Sed cement pastes achieved 0.810 and 0.815 respectively, while the strength of both mortars was 55.08 MPa and 56.57 MPa respectively. The porosity and critical diameter of the pores of both mortars were nearly identical at any time of testing.
(3) The modeling results of CEMHYD3D model also indicated that the DoH and cumulative hydration heat of OPC-Sed cement were higher than those of OPC Ref cement as indicated by the experimental results. This confirmed that the sediment substitution in the raw meal did not affect the reactivity of clinker phases.
(4) The hydration progress of individual cement phases as a function of time could be monitored in CEMHYD3D. The modeling result indicated that the hydration kinetics of individual cement phases were not similar. Indeed, the hydration of gypsum, C_3A and C_4AF phases begins much earlier than that of silicate phases (C_3S, C_2S). However, the length of the induction period in these phases was greater than that of the C_3S phase. The model result also indicated that total gypsum and C_3A phases were consumed after 28 days of curing and this was also confirmed by XRD analysis. The hydration rate of C_4AF was higher than that of silicate phases at very early ages, but much lower at long-term.
(5) The amount of some hydration products such as C-S-H gels, $Ca(OH)_2$ could be predicted in the CEMHYD3D. As expected, for the two cement pastes, the amounts of all hydration products were nearly similar. However, in the CEMHYD3D, the content of ettringite has decreased with an increase in the content of mono-sulfoaluminate, while the presence of both hemi-caboaluminate and mono-carboaluminate was not predicted. This was contrary to the XRD analysis result for the two cement pastes.
(6) As the experimental results on the mechanical-microstructural properties showed, the CEMHYD3D model also showed that the compressive strength of OPC-Sed mortar was slightly higher than that of the reference. However, it can be seen that the model result for the compressive strength was slightly higher than the experiment for both cements, while the porosity predicted in the CEMHYD3D was limited to the capillary porosity.

The findings of this study suggest promising results for future studies. The feasibility of recycling the sediment in the raw meal at an adequate rate could be applied on an industrial scale. Indeed, all the raw materials used in this study were also used on the industrial scale, so this study can provide a solid foundation for future work on an industrial scale. The modeling results also demonstrated the numerous advantages of using the CEMHYD3D for studying the hydration kinetics as well as mechanical-microstructural development of cement produced from the waste substitution in the raw meal. Based on the results obtained in this study, the CEMHYD3D can be used as a practical, reliable and economical tool for physical analyses of Portland cement hydration in a practical application with several cautions including the predicted porosity, conversion of ettringite to mono-sulfoaluminate, and formation of hemi-carboaluminate, mono-carboaluminate phases. In addition, the 3D-microstructure created in the CEMHYD3D was limited to 100 x 100 x 100 μm^3, the authors highly recommend that the cement used for the simulation has a smaller particle size than the critical diameter (30 μm) to ensure a good agreement with the experimental results.

Data availability

All results are available in the database. If it is necessary, please contact us at the following address: duc.chinh.chu@imt-nord-europe.fr

Code availability: CEMHYD3D: A Three-Dimensional Cement Hydration and Microstructure Development Modelling Package. Version 2.0 | NIST.

Funding sources

Research carried out within the framework of Project SEDICIM, financed by the FEDER funds.

Authorship contribution statement

Duc Chinh Chu: Conceptualization, Methodology, Investigation, Visualization, Writing-original draft.

Mahfoud Benzerzour: Methodology, Conceptualization, Supervision, Validation, Writing-review & Editing.

Joelle Kleib: Methodology, Conceptualization, Supervision, Validation, Writing-review & Editing.

Mouhamadou Amar: Methodology, Conceptualization, Supervision, Validation, Writing-review & Editing.

Nor-Edine Abriak: Methodology, Conceptualization, Supervision, Validation, Writing-review & Editing.

Guillaume Potier: Methodology, Conceptualization.

Jaouad Nadah: Methodology, Conceptualization, Supervision, Validation, Writing-review & Editing.

Declaration of competing interest

The authors of this article declare that they have no financial, professional or personal conflicts of in-terest that could have inappropriately influenced this work.

REFERENCES

1. Gao T, Shen L, Shen M, Liu L, Chen F. 2016. Analysis of material flow and consumption in cement production process, J. Clean. Prod. 112(1):553–565. https://doi.org/10.1016/j.jclepro.2015.08.054.
2. Roskos C, Cross D, Berry M, Stephens J. 2011. Identification and verification of self-cementing fly ash binders for “green” concrete. World of Coal Ash (WOCA) Conference.
3. National Minerals Information Center. 2013. Mineral commodity Summaries. U.S.G.S. U.S. Geological Survey. Retrieved From http://minerals.usgs.gov/minerals/pubs/mcs/.
4. Elchalakani M, Aly T, Abu-aisheh E. 2014. Sustainable concrete with high volume GGBFS to build Masdar City in the UAE. Case Stud. Constr. Mater. 1:10–24 https://doi.org/10.1016/j.cscm.2013.11.001.
5. Snellings R, Horckmans L, Van Bunderen C, Vandewalle L, Cizer Ö. 2017. Flash-calcined dredging sediment blended cements: effect on cement hydration and properties, Mater. Struct. 50:241. https://doi.org/10.1617/s11527-017-1108-5.
6. Benzerzour M, Maherzi W, Amar MAA, Abriak NE, Damidot D. 2018. Formulation of mortars based on thermally treated sediments. J. Mater. Cycles Waste Manag. 20:592–603. https://doi.org/10.1007/s10163-017-0626-0.
7. Chu DC, Amar M, Kleib J, Benzerzour M, Damien B, Abriak N, Jaouad N. 2022. The pozzolanic activity of sediments treated by the flash calcination method. Waste Biomass Valorization. 13:4963–4982. https://doi.org/10.1007/s12649-022-01789-8.
8. Amar M, Benzerzour M, Kleib J, Abriak N-E. 2021. From dredged sediment to supplementary cementitious material: characterization treatment and reuse. Int. J. Sediment Res. 36(1):92-109. https://doi.org/10.1016/j.ijsrc.2020.06.002.
9. Chu DC, Kleib J, Amar M, Benzerzour M, Abriak N. 2022. Recycling of dredged sediment as a raw material for the manufacture of Portland cement – Numerical modeling of the hydration of synthesized cement using the CEMHYD3D code. J. Build. Eng. 48:103871. https://doi.org/10.1016/j.jobe.2021.103871.
10. Aouad G, Laboudigue A, Gineys N, Abriak NE. 2012. Dredged sediments used as novel supply of raw material to produce Portland cement clinker. Cem. Concr. Compos. 34(6):788–793. https://doi.org/10.1016/j.cemconcomp.2012.02.008.
11. Faure A, Coudray C, Anger B, Moulin I, Colina H, Izoret L, Théry F, Smith A. 2019. Beneficial reuse of dam fine sediments as clinker raw material. Constr. Build. Mater. 218:365–384, https://doi.org/10.1016/j.conbuildmat.2019.05.047.
12. Bentz D. 2005. CEMHYD3D: A three-dimensional cement hydration and microstructure development modeling package. Version 3.0. NIST Interagency/Internal Report (NISTIR), National Institute of Standards and Technology, Gaithersburg, MD. https://doi.org/10.6028/NIST.IR.7232.
13. Bentz DP. 2006. Capillary porosity depercolation/repercolation in hydrating cement pastes via low-temperature calorimetry measurements and CEMHYD3D modeling. J. Am. Ceram. Soc. 89(8):2606–2611. https://doi.org/10.1111/j.1551-2916.2006.01102.x.
14. Bentz DP, Feng X, Haecker CJ, Stutzman PE. 2000. Analysis of CCRL proficiency cements 135 and 136 using CEMHYD3D. NISTIR 6545. National Institute of Standards and Technology (NITS). Retrieved from https://www.researchgate.net/publication/240236886_Analysis_of_CCRL_Proficiency_Cements_135_and_136_Using_CEMHYD3D.
15. Bentz DP, Ferraris CF, Jones SZ, Lootens D, Zunino F. 2017. Limestone and silica powder replacements for cement: Early-age performance Cem. Concr. Compos. 78:43–56. https://doi.org/10.1016/j.cemconcomp.2017.01.001.
16. Bentz DP, Jensen OM, Hansen KK, Olesen JF, Stang H, Haecker CJ. 2004. Influence of cement particle-size distribution on early age autogenous strains and stresses in cement-based materials. J. Am. Ceramic Soc. 84(1):129-135. https://doi.org/10.1111/j.1151-2916.2001.tb00619.x.
17. Bullard JW, Stutzman PE, Ordoñez Belloc LM, Garboczi EJ, Bentz DP. 2009. Virtual cement and concrete testing laboratory for quality testing and sustainability of concrete. Conference: Modeling as a Solution to Concrete Problems. ACI SP-266. Retrieved from https://www.researchgate.net/publication/241196517_Virtual_Cement_and_Concrete_Testing_Laboratory_for_Quality_Testing_and_Sustainability_of_Concrete.
18. Bullard JW, Ferraris CF, Garboczi EJ, Martys N, Stutzman PE. 2000. User’s guide to the NIST virtual cement and concrete testing laboratory, Version 1.0. Retrieved from https://www.nist.gov/publications/users-guide-nist-virtual-cement-and-concrete-testing-laboratory-version-10.
19. van Breugel K. 1995. Numerical simulation of hydration and microstructural development in hardening cement-based materials (I) theory. Cem. Concr. Res. 25(2):319–331. https://doi.org/10.1016/0008-8846(95)00017-8.
20. Qi T, Zhou W, Liu X, Wang Q, Zhang S. 2021. Predictive hydration model of Portland cement and its main minerals based on dissolution theory and water diffusion theory. Materials. 14(3):595. https://doi.org/10.3390/ma14030595.
21. Bullard JW. 2007. Approximate rate constants for nonideal diffusion and their application in a stochastic model. J. Phys. Chem. A. 111(11):2084–2092. https://doi.org/10.1021/jp0658391.
22. Thomas JJ, Biernacki JJ, Bullard JW, Bishnoi S, Dolado JS, Scherer GW, Luttge A. 2011. Modeling and simulation of cement hydration kinetics and microstructure development. Cem. Concr. Res. 41(12):1257–1278. https://doi.org/10.1016/j.cemconres.2010.10.004.
23. Liu C, Wang F, Zhang M. 2020. Modelling of 3D microstructure and effective diffusivity of fly ash blended cement paste. Cem. Concr. Compos. 110:103586. https://doi.org/10.1016/j.cemconcomp.2020.103586.
24. Taylor HFW. 1998. Cement chemistry. Second edition. Ed. Thomas Telford. London.
25. Schläpfer P, Bukowski R. Untersuchungen über die bestimmung des freien kalkes und des kalziumhydroxydes in zement-klinkern zementen schlacken und abgebundenen hydraulischen mörteln eidgenössische materialprüfungsanstalt an der E.T.H, in Zürich, 63.
26. Bogue RH, Lerch W. 1934. Hydration of portland cement compounds. Ind. Eng. Chem. 26(8):837–847. https://doi.org/10.1021/ie50296a007.
27. Anger B. 2015. Caractérisation des sédiments fins des retenues hydroélectriques en vue d’une orientation vers des filières de valorisation matière. Conférence Méditerranéenne Côtière et Maritime Edition 3, Ferrara, Italia (2015). Retrieved from https://www.paralia.fr/cmcm/e03-20-anger.pdf.

28. Zaki M, Sharma S, Gurjar SK, Goyal R, Jayadeva Krishnan NMA. 2023. Cementron: machine learning the alite and belite phases in cement clinker from optical images. Constr. Build. Mater. 397:132425. https://doi.org/10.1016/j.conbuildmat.2023.132425.
29. Association Française de Normalisation (AFNOR). NF EN 197-1. 2012. Composition spécifications et critères de conformité des ciment courant.
30. Association Française de Normalisation (AFNOR). NF EN 196-6. 2018. Méthodes d'essai des ciments - Détermination de la finesse.
31. Association Française de Normalisation (AFNOR). NF EN 196-3. 2009. Methods of testing cements, Part 3 – Determination of setting times and soundness.
32. Dalton JL, Gardner KH, Seager TP, Weimer ML, Spear JCM, Magee BJ. 2004 Properties of Portland cement made from contaminated sediments. Resour. Conserv. Recycl. 41(3):227–241. https://doi.org/10.1016/j.resconrec.2003.10.003.
33. Chu DC, Kleib J, Amar M, Benzerzour M, Abriak N-E. 2021. Determination of the degree of hydration of Portland cement using three different approaches: Scanning electron microscopy (SEM-BSE) and Thermogravimetric analysis (TGA). Case Stud. Constr. Mater. 15:e00754. https://doi.org/10.1016/j.cscm.2021.e00754.
34. Bullard JW, Evans DL, Bond PJ. 2003. The virtual cement and concrete testing laboratory consortium. Annual Report 2003.
35. Scrivener K, Snellings R, Lothenbach B. 2016. A practical guide to microstructural analysis of cementitious materials. Ed. Taylor & Francis Group. Crc Press Boca Raton F.L. USA.
36. Association Française de Normalisation (AFNOR). NF EN 196-1. 2016. Méthode d'essai des ciments- Partie 1: Détermination des résistance.
37. British Standards BS 1881: Part 124. 1988. British standard testing concrete. Part 124. Methods for analysis of hardened concrete.
38. Bentz DP. 2006. Modeling the influence of limestone filler on cement hydration using CEMHYD3D. Cem. Concr. Compos. 28(2):124–129. https://doi.org/10.1016/j.cemconcomp.2005.10.006.
39. Bentz DP. 1997. Guide to using CEMHYD3D: A three-dimensional cement hydration and microstructure development modelling package. National Institute of standards and technology. Retrieved from https://www.researchgate.net/publication/237062671_Guide_to_using_CEMHYD3D_A_three-dimensional_cement_hydration_and_microstructure_development_modelling_package.
40. Bentz DP, Ferraris CF, Galler MA, Hansen AS, Guynn JM. 2012. Influence of particle size distributions on yield stress and viscosity of cement-fly ash pastes. Cem. Concr. Res. 42(2):404–409. https://doi.org/10.1016/j.cemconres.2011.11.006.
41. Beaudoin J, Odler I. 2019. Hydration setting and hardening of Portland cement. Elsevier Ltd.
42. Jansen D, Goetz-Neunhoeffer F, Stabler C, Neubauer J. 2011. A remastered external standard method applied to the quantification of early OPC hydration. Cem. Concr. Res. 41(6):602–608. https://doi.org/10.1016/j.cemconres.2011.03.004.
43. Bullard JW, Jennings HM, Livingston RA, Nonat A, Scherer GW, Schweitzer JS, Scrivener KL, Thomas JJ. 2011. Mechanisms of cement hydration. Cem. Concr. Res. 41(12):1208–1223. https://doi.org/10.1016/j.cemconres.2010.09.011.
44. Zhang Z, Scherer GW, Bauer A. 2018. Morphology of cementitious material during early hydration. Cem. Concr. Res. 107:85–100. https://doi.org/10.1016/j.cemconres.2018.02.004.
45. Richardson IG. 1999. Nature of C-S-H in hardened cements. Cem. Concr. Res. 29(8):1131–1147. https://doi.org/10.1016/S0008-8846(99)00168-4.
46. Antoni M, Rossen J, Martirena F, Scrivener K. 2012. Cement substitution by a combination of metakaolin and limestone. Cem. Concr. Res. 42(12):1579–1589. https://doi.org/10.1016/j.cemconres.2012.09.006.
47. Matschei T, Lothenbach B, Glasser FP. 2007. The role of calcium carbonate in cement hydration. Cem. Concr. Res. 37(4):551–558. https://doi.org/10.1016/j.cemconres.2006.10.013.
48. Matschei T, Lothenbach B, Glasser FP. 2007. The AFm phase in Portland cement. Cem. Concr. Res. 37(2):118–130. https://doi.org/10.1016/j.cemconres.2006.10.010.
49. De Weerdt K, Haha M, Ben Le Saout G, Kjellsen KO, Justnes H, Lothenbach B. 2011. Hydration mechanisms of ternary Portland cements containing limestone powder and fly ash. Cem. Concr. Res. 41(3):279–291. https://doi.org/10.1016/j.cemconres.2010.11.014.
50. Roy DM. Concrete: by Sidney Mindess and J, Francis Young, Prentice-Hall Inc, Englewood Cliffs.
51. Zhang S, Zhang M. 2006. Hydration of cement and pore structure of concrete cured in tropical environment. Cem. Concr. Res. 36(10):1947–1953. https://doi.org/10.1016/j.cemconres.2004.11.006.